Soft Matter

Role of Ionic Interactions in Deformation and Fracture Behavior of Perfluorosulfonic-acid Membranes

Journal:	*Soft Matter*
Manuscript ID	SM-ART-09-2019-001964.R1
Article Type:	Paper
Date Submitted by the Author:	02-Dec-2019
Complete List of Authors:	Shi, Shouwen; Lawrence Berkeley National Laboratory, Energy Storage and Distributed Resources; Tianjin University, School of Chemical Engineering and Technology Liu, Zheng; Tianjin University, School of Chemical Engineering and Technology Lin, Qiang; Tianjin University, School of Chemical Engineering and Technology Chen, Xu; Tianjin University, School of Chemical Engineering and Technology Kusoglu, Ahmet; Lawrence Berkeley National Laboratory, Energy Storage and Distributed Resources

Role of Ionic Interactions in Deformation and Fracture Behavior of Perfluorosulfonic-acid Membranes

Shouwen Shi,[a,b] Zheng Liu, [a] Qiang Lin, [a] Xu Chen[a] and Ahmet Kusoglu[b,*]

[a] School of Chemical Engineering and Technology, Tianjin University, Tianjin 300072, China

[b] Energy Storage and Distributed Resources Division, Lawrence Berkeley National Laboratory

1 Cyclotron Road, Berkeley CA 94720, USA

*Corresponding author. E-mail address: akusoglu@lbl.gov

Abstract

The stability of ion-conductive membranes, such as perfluorosulfonic-acid (PFSA), as a solid-electrolyte separator in energy devices is strongly linked to their mechanical properties, characterization of which presents challenges, especially in the presence of ionic interactions. Ionomer membranes' elastic properties are affected by cations, however, their influence on deformation at small and large strains are relatively unexplored. In this paper, we report the stress-strain response and fracture behavior of Nafion membranes exchanged with various cations examined in three deformation regimes. In small-strain regime, Young's modulus is strongly dependent on cation size, due to reduced mobility and local stiffening of the polymer chains. Young's modulus, yield limit and strain-hardening modulus all increase with monovalent cation size in the order: $H^+ < Li^+ < K^+ < Na^+ < Cs^+$, but with varying dependence. In the failure regime, however, break strain and fracture energy of the membrane decreases in the

presence of larger cations, which promote deformation instability while decreasing plastic dissipation energy during crack propagation, thereby leading to more brittle fracture. These results not only demonstrate the trade-off between strength and fracture toughness, but also reveal how it is altered by the ionic interactions, which also dictate the inverse relationship between stretchability and stiffness. Moreover, the measured stress-strain data are reproduced by the constitutive relations to extract parameters that are correlated to the fracture energy through craze instability. Such relationships provide insight into how parameters extracted from tensile testing can be used to assess membrane stability and the role of ionic interactions.

Keywords: PFSA membranes; Cations; Mechanical property; large-strain deformation; fracture toughness; constitutive relations

1. Introduction

Ion-conductive polymers, or ionomers, are a key component in electrochemical energy conversion devices where they function as a separator and a solid-electrolyte membrane. While the former functionality is critical to insulate electrons and separate the species that react in the electrodes, the electrolyte functionality enables selective transport of ions necessary to complete the reactions and is therefore directly linked to the device performance. Performance of the ionomers as solid-electrolyte is commonly associated with transport properties, whereas their stability as a separator is strongly linked to their mechanical stability. Thus, it is of interest to accurately characterize the mechanical stability of solid-electrolyte membranes with a range of mechanical properties and elucidate the factors controlling their interrelation.

One class of polymer-electrolyte that exhibits such multi-functionality is perfluorinated sulfonic acid (PFSA) ionomers, that are widely used in polymer-electrolyte fuel cells and electrolyzers, and redox flow batteries due to their exceptional selective ion transport properties and chemical-mechanical stability.[1, 2] This multi-functionality is accomplished within the ionomer's phase-separated nano-morphology comprised of hydrophilic ionic nano-domains facilitating ion transport, and the hydrophobic semi-crystalline matrix providing mechanical stability. PFSA consists of a chemically inert poly-tetrafluoroethylene (PTFE) backbone and side-chain terminated with hydrophilic sulfonic acid groups (SO_3^-). In protonated form, protons attached to PFSA's SO_3^- groups ($R\text{-}SO_3^- + H^+ \leftrightarrow SO_3H$) dissociate in the presence of water, thereby giving the ionomer its inherent, hydration-dependent proton conductivity.[2] The sulfonic acid groups solvated by water molecules form hydrophilic nano-domains, creating a phase-separated morphology and governing membrane's macroscopic properties through a structure-property relationship.[3, 4] This structure-property relationship and cation-transport properties are influenced by many factors, such as processing,[3, 5, 6] ageing and degradation [7, 8] and cationic interactions.[4, 9-19] While majority of the studies on PFSA are based on proton-form,[2] understanding the membrane behavior in other cation forms have always been of interest for it provides a new paradigm to alter and study the nature of ionic interactions and their impact on hydration and transport properties.

The effects of cation type on PFSA behavior manifest themselves through the ionic interaction between mobile cation and fixed anionic site, as well as the solvation energy between cation and solvent molecules, dielectric constant, dipole-dipole interactions, all of which ultimately alter the ionomer's local structure and macroscopic properties.[2, 12-15, 17, 19-23] Investigations on PFSAs in proton and other cation forms have provided insight into the ion transport mechanisms, such as water-mediated

ion transport and role of hydrogen bonding.[4, 10, 15, 17, 19, 21, 24-27] Impact of a cations associated with not only its interaction strength and mobility within the ionic region, but also the intermediate region occupied by the fluoroether side-chains, which affect the polymer-chain segmental motion and morphology.[2, 10, 19, 23, 28] To elucidate how these interactions influence ionomer behavior, many studies focused on measuring the properties of PFSA membranes exchanged with different cationic forms.[2, 4, 12, 13, 15, 19-23]

The role of cation in PFSA's structure-property relationship changes with the hydration level; while the ionic interactions impacted by cations are dominant at lower water hydration levels, their effect is shielded and diminished with the addition of water molecules that act like "free water" in aqueous solutions.[4, 29-32] Exchanging a proton with a larger cation changes the physical structure by creating transient ionic crosslinks, but introducing a multivalent cation of charge z creates stronger ionic crosslinks by coordinating with z $-SO_3^-$groups, per electroneutrality, which are effective especially at low hydration.[4, 13, 14, 16, 22, 29-31, 33, 34] Thus, these changes in the local environment upon cation exchange manifest themselves by altering the mobility of chains, ions, and other species, thereby affecting not only the membrane's transport functionality, but also its mechanical properties. While literature is abundant with studies on the impact of cation (exchange) on Nafion membrane's hydration[4, 13, 17, 18, 35-37] and transport properties,[4, 15, 16, 24-26, 34, 38-41] especially the changes in ion and water transport mechanisms, the studies relevant to mechanical properties are relatively scarce.

In addition to many studies on reporting mechanical properties of proton-form PFSA and their environmental dependence based on uniaxial tension tests[33, 42-49] and constitutive models,[43, 50, 51] a few studies investigated the effect of cations on Nafion's mechanical response.[30, 52-56] (see ref.[2] for a review of the topic). It has been reported that Young's moduli increases with the cation radius (r_c),[4, 52-54] and is

less affected by cation valance (*z*), which is ascribed to the surface area available to ionic moieties during physical crosslink formation.[4, 53, 54] The viscosity of Nafion studied using molecular dynamics (MD) simulations was found to be correlated with ionic crosslinks induced by sulfonate anion-cation and related to the size of crosslink networks.[57] In addition, fracture behavior of Nafion was studied to determine its temperature-dependent fracture toughness.[58, 59] Cations were shown to affect the mechanical behavior of catalyst-coated membranes as well.[54] The presence of water, however, reduces the difference between the tearing fracture energy of Nafion in proton-form and other cation forms, due to the shielding effect of water reducing the ionic interactions between cation and sulfonate anion. Similar observations were reported for stress relaxation behavior of cation–exchange Nafion, which was shown to change with cations in ambient conditions,[56] but found to be independent of the cation type in water.[30] Thus, the impact of ionic interactions on ionomer's mechanical response can be accessed better in dry state. Even though effect of cations on mechanical properties of PFSA have been reported, the underlying mechanisms controlling their stress-strain response and fracture behavior have not been fully understood. In particular, most studies in the ionomer literature focused on the elastic properties, with limited investigations on the post-yield region and plasticity, especially with the impacts of cations on properties such as toughness that are critical to the mechanical stability. The latter phenomenon could provide more information about the interplay between the ionic interactions, and chain deformation and mobility. Effect of ionic crosslinks on mechanical stability have been studied for ionomeric elastomers,[60] hydrogels and biological scaffolds,[61-66] but their impact on ionomers have been limited to systems such as sulfonated polystyrene.[67-70]

What remains to be elucidated in mechanical behavior of cation-exchanged PFSAs, and semi-crystalline ionomers in general, is the relationship among various measured mechanical properties, in an

attempt to link stress-strain response and fracture toughness, and thus moving beyond elastic properties and membranes in proton form. Hence, the objective of this paper is to present an in-depth analysis of the mechanical response of Nafion, from low-strain to large-strain deformation to fracture behavior, identify the key mechanical properties and elucidate how their underlying interrelations are affected by the cationic interactions.

2. Experimental

2.1 Membrane Preparation

In this study, Nafion® 212 membranes were purchased in protonated (H^+) form from Ion Power Inc. (New Castle, DE) with the nominal thickness of 50 µm. Membranes were soaked into 0.5M (Li_2SO_4, Na_2SO_4, K_2SO_4, Cs_2SO_4, $Fe_2(SO_4)_3$ and 1M ($MgSO_4$, $CuSO_4$, $ZnSO_4$, $FeSO_4$) aqueous sulfate solutions (from Sigma Aldrich and J.T. Baker) for 48 to 72 hours under ambient conditions to achieve new cationic forms, using the same procedure as described in a previous study.[4] The size of the membrane specimens, the volume of salt solutions and the amount of soak time were carefully selected to make sure that protons in membranes were fully exchanged with cations, as described previously.[71] Then, the membrane specimens were rinsed in deionized water for 3 times to remove excess solution on surface and stored in deionized water until use. The membranes were dried in vacuum oven at 60°C for at least 12 hours before testing.

2.2 Mechanical Testing

Uniaxial tests were carried out using a tensile testing machine (Instron) at room condition (25°C and *ca.* 50% RH). Rectangular specimens with the gauge length of 60 mm and width of 12 mm were used. Uniaxial tensile tests were conducted under strain control with a strain rate of 0.001 s^{-1}. The specimens

were stretched until it breaks, and the final break stress and strain were recorded (Figure 1). To ensure reproducibility, at least two samples were repeated for each condition.

2.3 Dynamic Mechanical Analysis

The dynamic mechanical properties of different cationic Nafion membrane are measured using a dynamic mechanical analyzer (DMA) (Tritec 2000). Specimens were cut into rectangular piece with the gauge length of 10 mm and width of 7 mm. They were tested in tension mode with the frequency of 1 Hz. Temperature was ramped from room temperature to 400 °C with a heating rate of 5°C/min. The alpha-relaxation temperature, T_α, was determined from the peak in tan(δ) during temperature sweep, and the storage moduli are measured at different temperatures, including after T_α, which corresponds to the rubbery modulus, as discussed in ref.[4] The rubbery modulus was determined as the storage modulus after reaching the alpha-relaxation temperature.

2.4 Double Edge Notch Tension Test

Membranes were cut into rectangular strips with the length of 40 mm and width of 20 mm. Before testing, double edge notch tension (DENT) specimens were prepared by cutting along the width direction from edges using a fresh razor blade. The remaining length is termed as the *ligament length, l*. In this study, the fracture behaviors of membranes with the ligament length ranging from 5 to 12 mm were investigated on an *in-situ* tensile testing machine (IPBF-300, CARE Measurement & Control Co., Ltd, China). The resulting load-displacement and variation in crack length during crack propagation were continuously captured, as illustrated in Figure 1. Detailed description can be found in our previous work.[72] The double edge notch tension tests were performed at room condition (23±1°C, 50% RH).

3. Results and Discussion

Mechanical testing methods employed in this study are depicted in Figure 1, along with the schematic descriptions of the mechanical properties that can be determined for each deformation mode, namely, small-strain and large-strain deformation, and fracture behavior. In addition, list of mechanical properties that can be extracted from these tests are summarized in detail in Table 1 and will be discussed through the text.

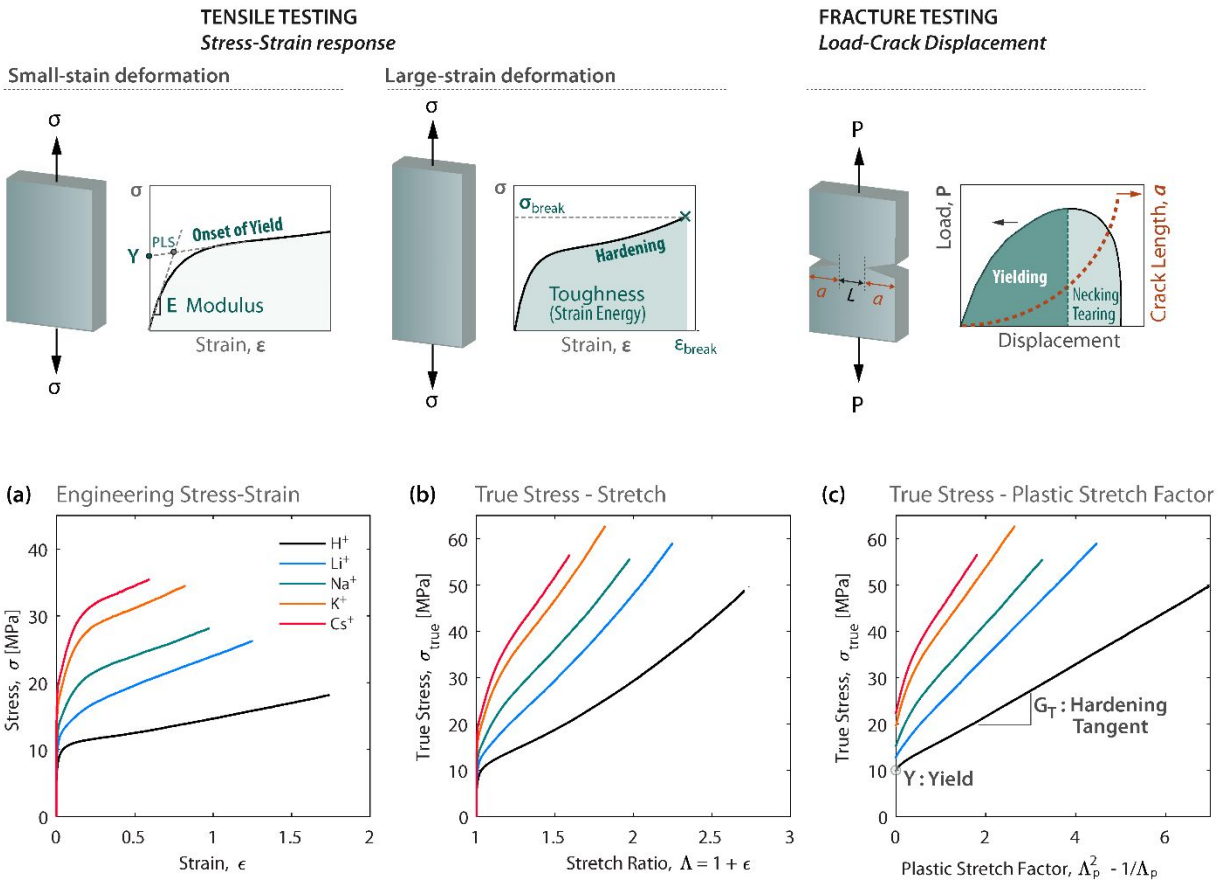

Figure 1 Schematic description of mechanical testing of a polymer membrane in small- and large-strain deformation mode as well as in fracture failure mode, shown with the key mechanical properties that can represent various deformation mechanisms. Uniaxial tensile properties of Nafion 212 membranes in different cationic shown in the form of: (a) engineering stress-strain response, (b) true stress-stretch and (b) true stress-plastic stretch factor.

Table 1 List of mechanical properties that can be extracted from stress-strain and fracture tests as well as constitutive modeling.

Parameter		Testing Mode	Units	Description
E	Young's modulus	Small-strain tensile testing	MPa	Slope of initial linear stress-strain
Y	Yield Limit		MPa	Stress at zero plastic strain (or elastic strain limit, ε_0)
Y/E	Strength-to-Stiffness Ratio		[Strain]	Elastic strain limit, ε_0, where Y is set
PLS	Proportional Limit Stress		MPa	Intersection of initial linear and hardening tangent (PLS ~ Y)
$\mathbf{G_T}$	Hardening Tangent	Large-strain tensile testing	MPa	Slope of true stress-stretch factor
$\mathbf{Y/G_T}$	Instability Factor		[Strain]	Characterizes plastic deformation and crack/craze instability
$\boldsymbol{\sigma_{break}}$	Break Stress		MPa	Maximum stress at break
$\boldsymbol{\varepsilon_{break}}$	Break Strain		[Strain]	Elongation to break (Stretchability)
$\mathbf{w_f}$	Fracture Toughness	Fracture Testing (DENT)	MPa.mm	Intrinsic Fracture energy, independent of ligament (crack) size
$\boldsymbol{\beta w_p}$	Dissipation Energy		MPa	Plastic energy dissipation in outer crack zone

3.1 Uniaxial Tension Behavior

The stress-strain responses of Nafion membranes in different cationic forms are shown in Figure 1(a) in terms of engineering stress and strain. It follows from the figure that as the size of the monovalent cation increases, from H^+ to those in alkali metal groups (Li^+, Na^+, K^+, Cs^+), there is a clear shift in membrane stress-strain response towards higher initial stiffness (E) and yield stress, but with reduced break strain, ε_{break}. In addition, the transition from initial elastic regime to strain-hardening becomes more pronounced with increasing cation size. Thus, the influence of cations on deformation behavior differs in the post-yield regime, where the polymer chains align themselves in the direction of applied load. From a molecular perspective, the small-strain deformation corresponds to rotation of mesoscopic aggregates of polymer nano-domains, whereas the large deformation corresponds to alignment of polymer chains and aggregates within this mesoscale network.[73, 74] Such nanostructural orientation occurring in proton-form PFSA membranes during stretching was associated with preferential alignment of the polymeric aggregates in the direction of applied load.[74-78] This nanostructural anisotropy was observed also in Na^+ form,[79] and shown to induced anisotropy in transport properties as well.[76, 79, 80] In what follows below, various mechanical properties listed in Table 1 will be determined from Figure 1 and discussed in terms of governing phenomena.

3.2 Small-Strain Deformation

Young's moduli, E, calculated from the initial slope of tensile stress-strain curves increases with increasing cation size (radius) for monovalent cations, in agreement with previous observations.[4, 54] The deviation in Young's modulus due to multivalent cations is much smaller compared to significant increase in E with monovalent cation size, as shown in Figure 2. Similar observations are also reported by Jia *et al*. [54] at 23°C and 80°C and Kundu *et al*.[53] Young's modulus increases with increasing ion radius,

$E \propto r_c$, which is attributed to the increased restrictions on polymer chain motion in the presence of larger cations.[4, 54]

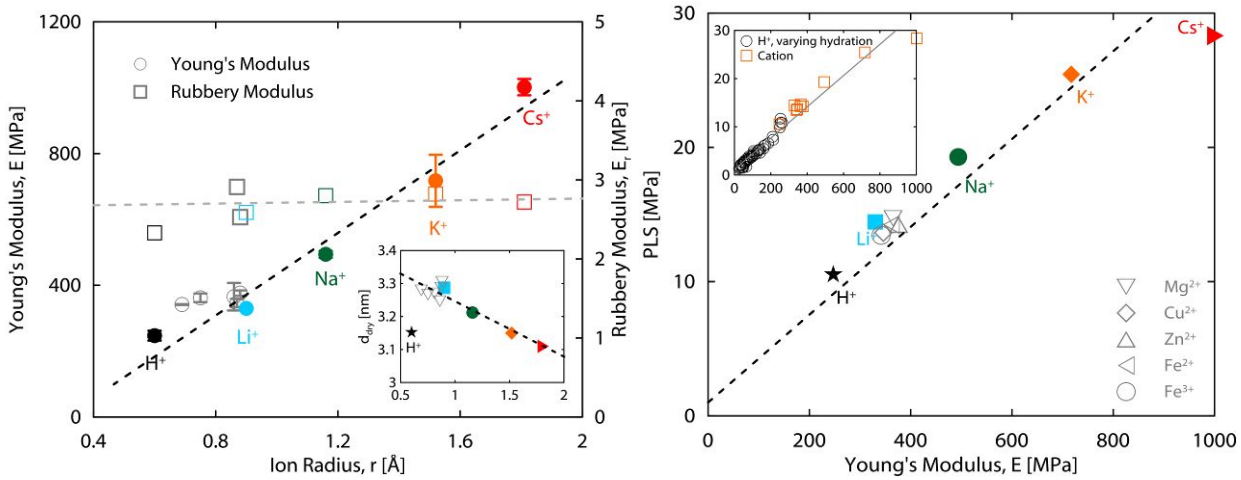

Figure 2 (a) Young's modulus and rubbery modulus of cation-exchanged Nafion. The inset shows the relationship between dry domain spacing, d_{dry} and cation radius (from ref.[4]). (b) Relationship between proportional limit stress (PLS) and Young's modulus in different cationic forms showing a representation of the strength-to-modulus ratio. The inset shows comparison of data for cation-exchanged Nafion (this work) and proton-form Nafion in different hydration states (from ref.[43, 49, 81]) Open gray symbols show the multivalent cations in both plots.

Larger cations not only hinder the mobility within ionic clusters, but also impose stronger restrictions on the segmental motion of the main-chain to which they are anchored. In fact, large cations could densify the local ionic regions, which can be deduced from the reduced domain spacing in the presence of larger cations, as inferred from SAXS (inset of Figure 2(a)).[4] In such a geometry, the concentration of ionic crosslinks per volume increases, which results in higher stiffness. Hence, Young's modulus increases proportional to the cation radius. A noteworthy observation is that modulus for multivalent cations also fall on the same trend set by the monovalent cations, which confirms the dominant role of cation size, more so than their charge, in small-strain deformation.

As it is not trivial to identify the onset of yielding from a tensile stress-strain curve, a proportional limit stress (PLS) describing the onset of nonlinearity is adopted first.[2, 43] The PLS is defined as the stress at the intersection of the tangents to the initial linear regime and the strain hardening regime of the curve[2, 82, 83] (Figure 1a). The PLS of Nafion also increases with increasing cation radius, in a similar fashion with Young's modulus. In fact, when PLS is plotted against Young's modulus, all data points fall on the same line regardless of the cation type (Figure 2). Such an inter-dependence implies an underlying deformation mechanism that governs both the elastic regime (modulus) and the onset of nonlinearity (PLS). Thus, assuming that PLS is a fair representation of the yield stress, σ_Y, the slope of this line can be interpreted as a strength-to-modulus ratio, $PLS/E \approx \sigma_Y/E$, a metric that can be interpreted as the elastic strain limit, $\varepsilon_0 = \sigma_Y/E = 0.03$. Moreover, a similar relationship between PLS and Young's modulus of Nafion can be obtained,[2] from the data measured at different temperature and relative humidity (RH) values.[2, 43, 49, 81] Our data extend this relationship to other cation forms, revealing that the elasticity and yielding can be described by a similar mechanism related to the small-strain deformation of polymer aggregates within the ionomer network. In particular, exchanging proton with other cations increases both PLS and modulus by preserving the membrane's intrinsic strength-to-modulus ratio and elastic strain limit, $\varepsilon_0 = \sigma_Y/E$.

3.3 Large-Strain Deformation

3.3.1 Constitutive Model

Next, we will adopt a constitutive model to examine how cations alter large-strain deformation behavior of a Nafion membrane and identify the governing phenomena in terms of cation interactions. Haward and Thackray[84, 85] proposed a constitutive model for large-strain deformation of semi-crystalline polymers based on the notion that the strain-hardening modulus determined from tensile experiment at

room temperature is governed by the entanglement density, which is determined by rubbery plateau modulus, E_r, measured from melt rheology. The model is expressed mathematically as:

$$\sigma = Y + G_T\left(\Lambda_p^2 - {}^{1}\!/_{\Lambda_p}\right) \quad \Lambda_p = 1 + \varepsilon_p = 1 + \varepsilon - \varepsilon_0 \tag{1}$$

where Λ_p is the plastic stretch ratio, ε_p is the plastic strain, *Y* is the *yield limit* (at zero plastic strain) and G_T is the *hardening tangent (modulus)*. The plastic strain can be linked to total (measured) strain, ε, using the elastic strain limit, ε (see Figure 2). Notably, this model captures the large-strain deformation once the yield point (*Y*, ε) is determined and the plastic strain is calculated accordingly. It must be noted that yield limit extracted from this model gives very similar values to the PLS described in the preceding section (See Figure S1 in SI).

It was previously reported that the Haward-Thackray model could reproduce the stress-strain response of proton-form Nafion, in dry and hydrated state,[43] and PTFE.[86] To examine this model's ability to capture the large-strain deformation of cation-exchanged Nafion membrane, the engineering stress-strain data shown in Figure 1 are converted to true stress, $\sigma_{true} = \sigma\,(1+\varepsilon)$, and plotted as a function of stretch ratio, Λ_p, and stretch factor, $\Lambda_p^2 - 1/\Lambda_p$ (Figure 1b-c). In the latter plot, stress shows a linear increase with stretch factor with a slope representing the hardening tangent, G_T, which increases with increasing cation radius (Table S1).

For semi-crystalline polymers, the entangled network of polymer chains intertwined with the crystallites is the origin of strain hardening behavior, where further stretching of polymer chains begin to limit their mobility and ability to orient in the direction of applied load, thereby creating additional resistance to deformation, as shown for other polymers,[87] including PTFE [86, 88], in addition to PFSAs.[2, 43, 50] In PFSAs, it is primarily the crystallites that act as (physical) crosslinks within the ionomer's network and

imparting its stability.[2, 4, 73] However, introduction of cations induce ionic crosslinks by interacting with poly-anion sites.[2] Together, these physical crosslinks (crystallites) and ionic crosslinks create a local morphology that is physically similar to an entangled semi-crystalline polymer network in terms of deformation, but one that also resembles to double-network hydrogels, in terms of the role of ionic crosslinks. As the mobility of polymer chains between crosslinks is limited, the increased crosslink density increases the mechanical strength, as also observed in other sulfonated ionomers[67, 69, 70] and hydrogels[61, 63-66] in the presence of ions. Thus, strain-hardening of the PFSA is attributed to the higher resistance to deformation arising from the orientation of semi-crystalline polymer aggregates, the mobility of which is mediated further by the ionic interactions (Figure 3).

While the ionic interactions could be associated with the electrostatic interactions or dipole-dipole interactions, their true nature is more complex and influenced by a number of factors, including the cation-water interactions (*e.g.,* solvation shell of the cations, number of water molecules), ionomer-cation interactions (*e.g.,* interaction strength) as well as the local structure of ionomer (*e.g.*, distance between adjacent sulfonate anions).[2, 13, 15, 17, 19, 20, 89-92] The latter represents the inter-ionic group distance and depends on the conformation of the backbone and side-chain, which are altered upon ion-exchange. A consequence of this effect is the reduced spacing of the ionic domains in membrane (Figure 2b, inset).[4, 18, 93] Recently, Crothers et al.[94] demonstrated that ion partitioning and equilibrium in Nafion ionomers requires an ionic solvation framework that treats the solution-like non-idealities resulting from hydration, electrostatics, ion association, and physical interactions within and external to the ionomer's hydrophilic domains. Thus, ionic interactions in Nafion cannot be easily attributed to a single factor, even though the strength of these interactions scales with ionic radius, at least for monovalent cations studied herein, and Lewis acid strength (LAS) could be used as a proxy for ion radius. For this reason,

cation radius is used as the key descriptor in this study. For example, in the case of R-SO_3^-•Cs^+, the total radii of the ions becomes comparable to the separation length of the adjacent ions, which along with the low hydration number for Cs^+, cause significant deviations in local interactions. In fact, for this reason, Nafion-Cs^+ has been considered a special case and studied in several studies,[15, 17, 19, 20, 89, 90, 95, 96] which suggested Cs^+ and similar heavy cations are located within close proximity of the SO_3^- ions,[17, 19, 95] result in a denser local structure,[4, 17, 19] and strong association of the Cs^+ with its conjugated base (fixed ionic groups) exhibit covalent-bond like character.[15] The focus of this study is how these changes impact ionomer's mechanical behavior.

To further examine this role of ionic interactions, we measured true stress-stretch factor for Nafion exchanged with multivalent cations (Figure S3). Stronger ionic crosslinks formed by the divalent cations by bridging the multiple poly-anionic groups (*i.e.*, R- SO_3^- • M^{2+} • SO_3^- -R) (Figure 3). Interestingly, variation in mechanical response due to multivalent cations (charge effect) is smaller than that observed among the monovalent cations (size effect). In fact, most of the stress-strain curves for Nafion exchanged with multivalent cations is enclosed between the two curves formed by Li^+- and Na^+-form membrane. Considering the radii of the multivalent cations studied here are also between the radius of Li^+ and Na^+, suggests that deformation behavior is controlled more by the cation size than the valance, although the latter still has a contribution. Such an effect could be attributed to changes in the physical network of polymer aggregates, wherein their inter-connectivity of the aggregates is modulated by the ionic interactions. For instance, in a MD study, the connectivity of Na^+ system was found to be higher than that of Ca^{2+} system, despite the stronger crosslinks in the latter.[57] These factors collectively determine the viscosity and the strain-hardening behavior of PFSA, which is relatively comparable between different cations forms, as shown in Figure S3. Hence, our findings support the notion that

cation size result in a more pronounced change in large-strain deformation of ionomers than does the cation charge number, z.

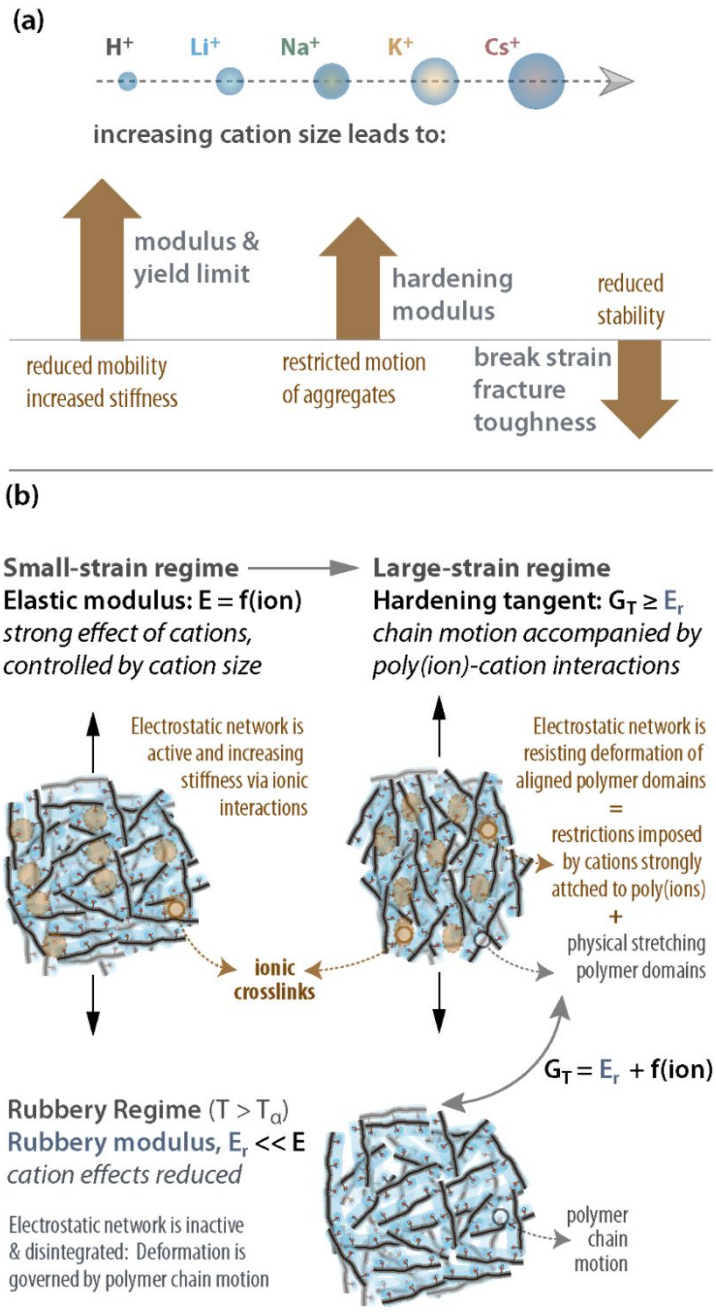

Figure 3 Pictorial description of deformation mechanisms in cation-exchanged PFSA ionomer membrane governing its stress-strain behavior in small-strain (elastic) regime and large-strain deformation (post-yield with hardening). Hardening modulus (G_T) of ionomer is characterized by contributions from stretching of polymer domains (represented by rubbery modulus, E_r) and ionic interactions (represented by a function, f(ion), which is inversely proportional to the cation radius).

3.3.2 Strain-Hardening Mechanism

Strain hardening can be characterized by either the *strain-hardening modulus*, E_H, extracted from the slope of stress-strain curve at larger strains (as shown in Figure 1), or the hardening tangent, G_T, described above. In the ensuing discussion, G_T will be used to represent hardening (Eq. (1)), noting its similar trend to the hardening moduli (*i.e.*, $G_T \sim E_H$) (Figure 4).

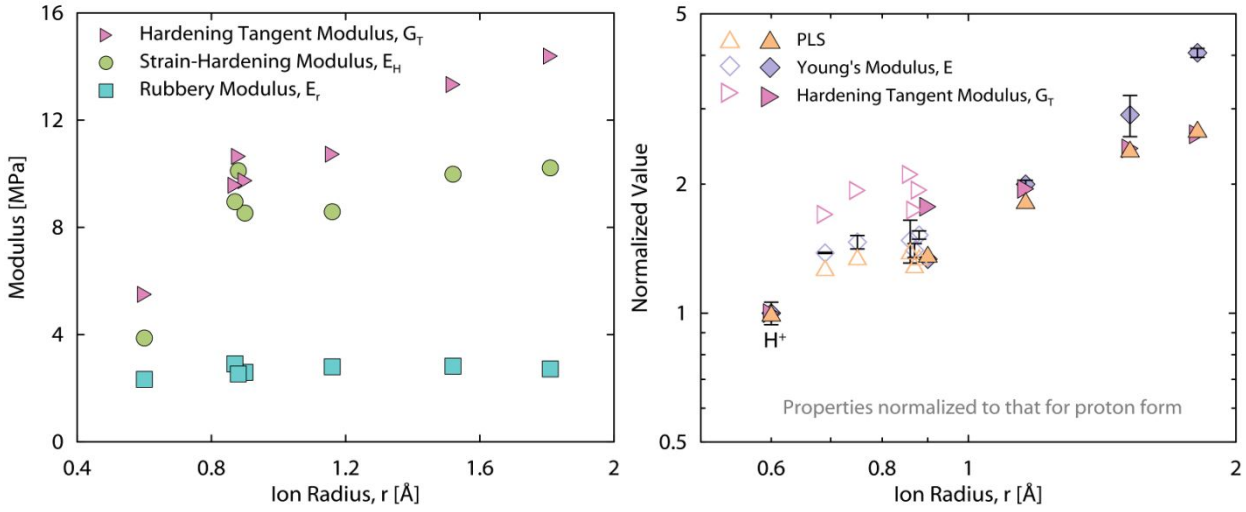

Figure 4 (a) Comparison of strain-hardening modulus, hardening tangent modulus and rubbery modulus as a function of ion radius. (b) Relative change in Young's modulus, PLS and hardening tangent moduli as a function of cation radius with respect to the reference values for H^+-form membrane. Data shown for monovalent cations (filled symbols) and multivalent cations (open symbols).

G_T is related to the network density in semi-crystalline polymers during plastic flow, the origins of which was proposed to be similar to the decrease in configurational entropy of polymer chains above their transition temperature.[84] To examine the physical meaning of the G_T in a PFSA, it is compared with modulus of membrane in rubbery state, E_r, obtained at a temperature higher than the ionomer's alpha-transition temperature (T_α), which marks the onset of destabilization of the ionic network.[97] For this reason, membrane rubbery modulus remains constant with no apparent dependence on the cation

radius, as shown in Figure 2(a), where the weakening of the ionic interactions mobilize the chains enough to facilitate their morphological rearrangement to overcome the restrictions imposed by the ionic crosslinks and interactions.[2, 4, 10, 98, 99] In the absence of ionic interactions, E_r account for only the entanglement density induced by physical crosslinks (Figure 3). E_r for Nafion is around 2.5 MPa, which is lower than G_T, but similar to equilibrium modulus value of 3 MPa reported by Patankar et al.[100, 101] based on long-term stress relaxation test and time-temperature superposition.

Figure 4a shows that while E_r remains constant, G_T increases with cation size, and the difference between the G_T and E_r then can be associated with the resistance driven solely by the ionic interactions during deformation. Thus, hardening behavior of Nafion is governed by the plastic flow of the polymer aggregates in the absence of ionic interactions (E_r), with an additional resistance caused by the interactions between poly-anions and cations ($G_T - E_r$) (Figure 3). The strength of this interaction between the sulfonate anion and cation increases for metal-alkali cations and multivalent cations, which can be quantified by either the cations radius the Lewis Acid Strength (LAS).[2, 4, 14, 102] The stronger the anion-cation interaction strength (e.g., as in R-SO_3^- • Cs^+), or the higher the cation size, r_c, the stronger their contribution to hardening via ionic crosslinks. This is demonstrated by the linear correlations between the hardening parameter ($G_T - E_r$) and LAS, which can be mathematically expressed as $G_T(ion) - E_r \propto r_c \propto 1/LAS$ (Figure 5). In the absence of any ionic interactions ($r_c \rightarrow 0$), the hardening behavior will be simplified to that of a system of polymer aggregates whose deformation is governed by entanglements and physical crosslinks. It must also be noted that, cations with large radius have lower surface charge density, which could weaken the distribution of interaction with fixed anions,[20] thereby underscoring the role of the physical size of the cations acting as inclusions from mechanics perspective. Hence, replacing protons with an alkali cation results in a convoluted impact on deformation; by

increasing the strength of ionic interactions and restricting local movement of aggregates through its size.

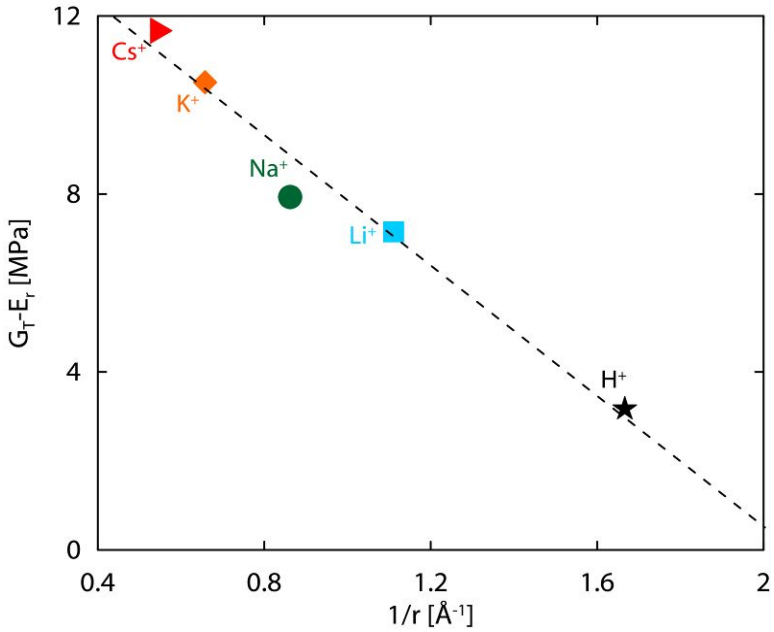

Figure 5 Difference between hardening modulus and rubbery modulus ($G_T - E_r$) plotted as a function of the cation's Lewis acid strength (inversely proportional to the cation radius) demonstrating the additional contribution from the larger cations with stronger ionic interactions to the hardening behavior of polymer during large-strain deformation.

Lastly, replacing H^+ with other cations in Nafion causes negligible change E_r (~10%) but result in a two-fold increase in G_T (Figure 4). This could be explained by the higher number of water molecules per ionic group, H_2O/SO_3^-, in H^+ form in the presence of a hydrogen-bonding network.[4] With the ease of dissociation and delocalization of protons ($R\text{-}SO_3H\bullet H_2O \rightarrow R\text{-}SO_3H{+}(H_2O)$), polymer chains in H^+-form membrane attain higher mobility and therefore could slide and extend with relatively less resistance during stretching. The fact that such increase occurs even for Li-form membranes, where the Li^+ radius is comparable to H^+, underscores the intriguing role of hydrogen bonds in reducing the ionomer's resistance to deformation at larger strains by facilitating chain motion and sliding (beyond yield point).

Our findings on the role of cations and H-bonded network on deformation of semi-crystalline ionomers complement studies on similar effects in deformation of amorphous hydrogels.[60, 103, 104]

A similar behavior is also observed for other glassy polymers which exhibit higher strain hardening modulus compared to rubbery modulus due to reduced chain mobility.[84, 105] When a polymer is stretched in the glassy state, a limited number of entropic configuration states is available for chains, in sharp contrast to the thermally-induced main-chain segmental mobility obtained in the rubbery state. Hence, the differences between hardening modulus and rubbery modulus of semi-crystalline polymers were attributed to their crystallinity, physical crosslinks and engagement density, as discussed in ref.[84] Our results herein lend credence to contribution by ionic crosslinks to deformation of an ion-containing semi-crystalline polymer below and above its transition temperature, which, in this case, is the ionic α-transition temperature, T_α.

3.4 Elongation to Break and Failure

Figure 6a shows that break strain, ε_b, decreases with increasing cation size (r_c) resulting an inverse relationship between E and the break strain, ε_b. Thus, a trade-off between modulus, E, and extensibility is observed for Nafion as shown in Figure 6(b), showing that an increase in stiffness of Nafion can be achieved via ionic crosslinks, but at the expense of reducing extensibility. This confirms the interrelation of extensibility (ductility) and modulus (stiffness); the stiffer the ionomer (due to cationic interactions), the lower its extensibility. Such a finding reveals the existence of a relationship between strength and ductility, which is an omnipresent phenomenon found in many materials, including metallic materials, ceramic materials, polymeric materials, composite materials and biological materials.[106, 107] In polymers, this trade-off is attributed to the interplay between the increasing flexibility of chains leading to low stiffness and high stretchability.[66, 86, 87, 108]

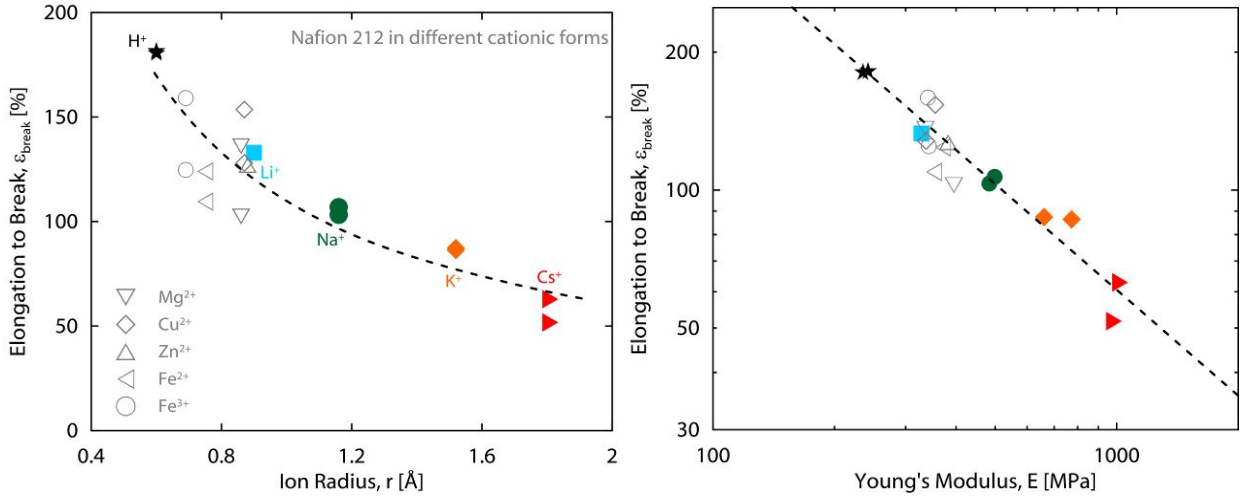

Figure 6 (a) Elongation to break of cationic Nafion membranes as a function of ion radius, r_c; (b) relationship between elongation to break and Young's modulus. Each data point represents a different measurement, and monovalent and multivalent cations are shown in filled and open symbols, respectively.

3.5 Fracture Behavior and Toughness

Toughness describes a material's resistance to fracture which also represents the deformation energy accumulated in the material during a tensile test. Hence, the area encompassed by stress-strain curve is integrated to determine the strain energy density $\Delta W^d = \int_0^{\varepsilon_{break}} \sigma d\varepsilon$, which represents toughness. Toughness of cation-exchanged Nafion membranes in dry state are comparable with a strain energy density value of ~25 MJ/m^3 (Figure S4). This is because the increase in strength with cation-driven restricted chain mobility is accompanied by a reduction in the break strain, which eventually leads to comparable strain-energy density values. The origin of mechanical toughness in dispersion-cast Nafion membrane is found to correlate best with the chain entanglement, instead of crystallinity.[109] Considering that cations have negligible impact on PFSA crystallinity,[4] underscores the role of network changes in deformation more than the semi-crystallinity.[4] Hitherto, only a few studies investigated the

underlying mechanisms controlling toughness in ionomers and the role of ionic interactions. Bellinger et al.[67] compared the tensile fracture properties of sulfonated polystyrene ionomers at low ion contents neutralized with different cations and found that replacing monovalent Na^+ ions by divalent Ca^{2+} ions resulted in a 37% increase in toughness. However, the difference between their experiments and this study is that the sulfonated polystyrene ionomers failed by craze formation at a very small strain of 3%, while the PFSA break at a much larger strain (>100 %) and possibly a different deformation mechanism. To examine the underlying nature of failure mechanisms, effect of cations on fracture behavior of Nafion is examined.

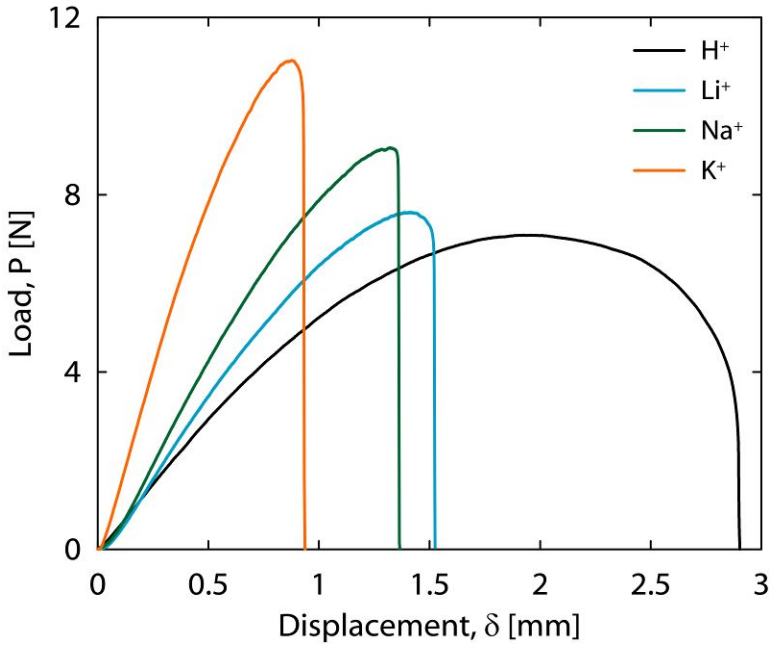

Figure 7 Load-displacement curves of Nafion membrane in monovalent cationic forms.

The load-displacement curves of Nafion membrane in different cationic forms at the same ligament length of 9.5 mm is shown in Figure 7. For H^+-form membrane, the load gradually decreases after reaching the maximum value, whereas for the other monovalent cationic membrane, the load exhibits a

sudden drop after reaching the maximum value. In addition, the larger the radius of the cation in Nafion, the higher the load and the smaller the displacement. As the maximum load point corresponds to ligament yielding, the maximum load follows a similar trend with the yield stress (Y). It should be noted that the maximum load point also corresponds to crack initiation, and the unloading part corresponds to crack propagation,[72] the sudden load drop of monovalent cationic membranes indicates a brittle fracture mode, whereas the gradually loading drop of H^+-form membrane indicates a ductile fracture mode.

To calculate the fracture resistance during crack initiation and propagation, the essential work of fracture (EWF) method is adopted where the contributions to the total fracture energy can be determined by collecting for various ligament (and crack) lengths. Detailed description of this method can be found in reference.[110] When the specific work of fracture is plotted as a function of ligament length, as shown in Figure 8, the intercept at zero ligament length, w_e, represents fracture toughness, while the slope βw_p corresponds to energy dissipated in the outer plastic zone. Thus, the fracture energy can be mathematically described as $w_f = w_e + \beta w_p$, corresponding to the energy dissipated for yielding and tearing, respectively (Figure 1). It can be observed from Figure 8b that the slope βw_p decreases with increasing cation radius, indicating smaller dissipated energy in the outer plastic zone, which corresponds to more brittle fracture mode. In H^+-form, ionomer shows the largest slope, and the higher intercept, which pinpoints a more ductile fracture behavior, where the hydrogen-bonded network likely helps maintain water molecules within their primary solvation shells and modulates dissipation of energy via plastic deformation (Figure 9). This change in fracture mode is confirmed by the examination of the fracture surfaces, which revealed distinct patterns: H^+-form membrane exhibits narrow striations almost parallel to crack growth direction, whereas these markings become wider and orient in

perpendicular direction for the membrane in Li^+, Na^+, or K^+ forms, indicating a transition from shear yielding to craze formation (Figure 9). Thus, fracture surface of the ionomer changes with increasing cation radius, in accordance with the faster crack propagation and brittle fracture mode.

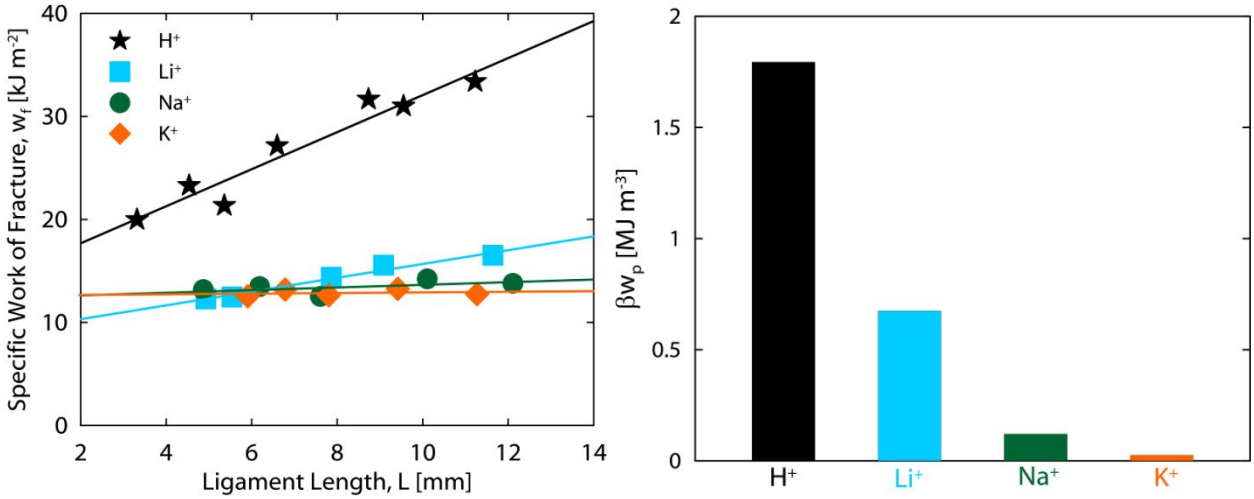

Figure 8 (a) Relationship between specific work of fracture and ligament length for membrane in different cationic forms. The solid lines are linear fitting to experimental data. (b) Comparison of βw_p for membranes in different cationic forms.

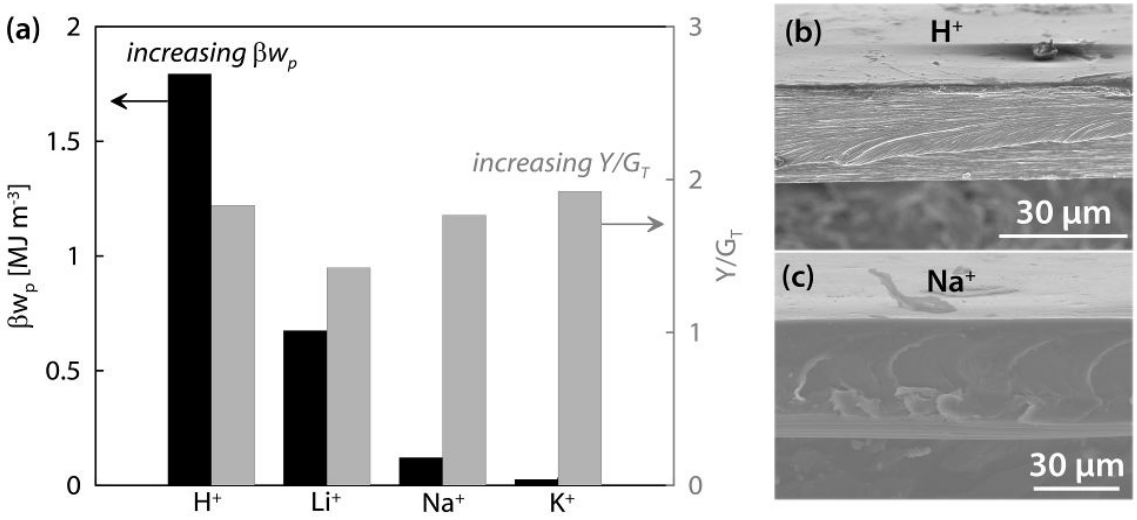

Figure 9 (a) Relationship between βw_p (dissipated energy from fracture tests) and Y/G_T (craze instability parameter from stress-stretch tests) for Nafion exchanged with various monovalent cations. Data are for Nafion in ambient conditions at 25°C. (b)-(c) are cross-section morphologies of H^+-form and Na^+-form membranes after DENT tests, respectively.

A few studies in the literature investigated the factors affecting fracture behavior of ionomers: Higher tensile strength and fracture energy of sulfonated polystyrene ionomers was reported upon changing cations from monovalent Na^+ to divalent Ca^{2+}, which was ascribed to the divalent cations' ability to form a stronger crosslinked network with higher stability of crazes, a precursor of crack.[67-69] A similar argument can be made for the ionomers studied herein to suggest that the craze stability in Nafion is controlled by cationic interactions, which govern large-strain deformation plasticity of the membrane. The interplay between the plastic deformation and fracture mode in cation-exchanged Nafion can be analyzed in light of crazing phenomenon. In polymers, *crazing*, is one of the precursors for crack and represents a region of highly localized plastic deformation of the polymer chains. Thus, a craze can be treated as an assembly of micro-necks with localized deformation. Therefore, break strain, to a large extent, governed by the stability of craze, which depends on the plastic stability and necking

behavior of the polymer.[85, 111] According to Haward and Thackray constitutive model (Eq. 1), for plastic instability and necking to occur, the *Considere's condition* should be achieved which gives $Y > 3G_T$.[85] The *Considere's condition* relates engineering stress to the conditions for necking, which gives $\Lambda_p \rightarrow 1, \frac{d\sigma}{d\Lambda_p} < 0$, where $\frac{d\sigma}{d\Lambda_p} = G_T\left(1 + \frac{2}{{\Lambda_p}^3}\right) - \frac{Y}{{\Lambda_p}^2}$. Under such condition, the ratio Y/G_T might be considered as the parameter to characterize the relative stability of craze; the larger the Y/G_T value, the lower the stability of the craze, as discussed in ref.[85] and also in Kramer's earlier works.[112, 113] Y/G_T for Nafion increases monotonically with the alkali cation radius, as shown in Figure 10a, where the for H^+-form membrane is an outlier with a relatively stable crack growth.

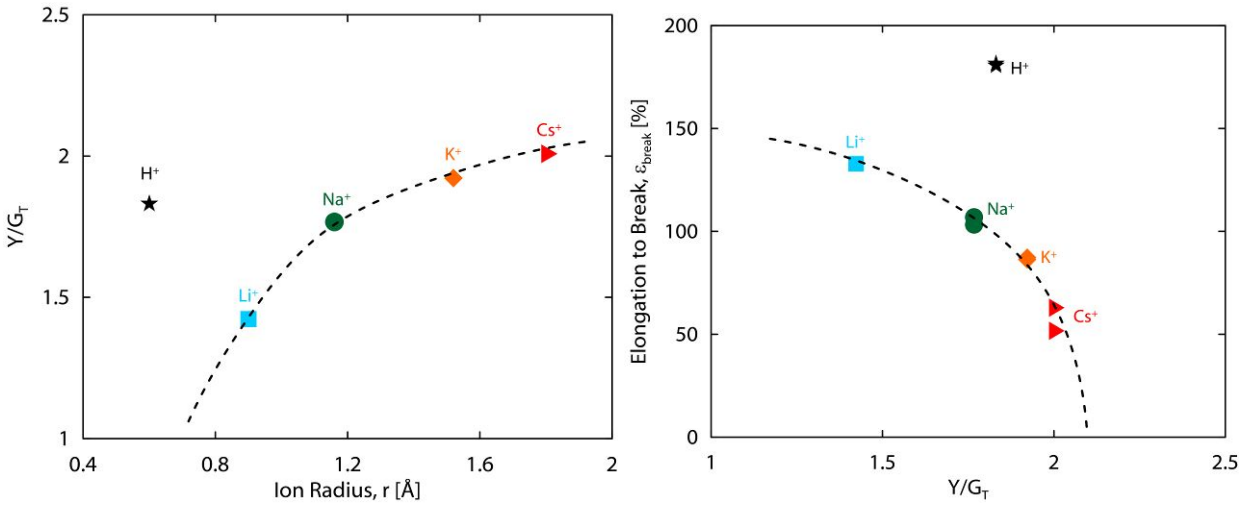

Figure 10 (a) Y/G_T as a function of cation radius; (b) relationship between break strain and Y/G_T for monovalent cations (filled symbols) and multivalent cations (open symbols).

Recalling that break strain also decreases with increasing cation size, a relationship between break strain and Y/G_T can be constructed (Figure 10b). The break strain decreases rapidly with increasing Y/G_T as the cation size increases in Nafion, which affirms that craze instability (*i.e.*, large Y/G_T) could be responsible for reduced extensibility. Even though the Y/G_T values are all smaller than 3, which is below

the critical value of plasticity instability, they can nevertheless be used as proxy for failure.[85, 87, 114, 115] In fact, origins of fracture in cation-exchanged Nafion can be better understood from examining the inverse relationship between βw_p and Y/G_T (Figure 9).

βw_p decreases with increasing Y/G_T, which corroborate that the ionomer dissipates reduced energy in the outer plastic zone of the crack, in accord with increasing craze instability (Y/G_T). In the presence of large cations interacting strongly with the sulfonate anions, the ionomer's ability to dissipate its energy through plastic deformation and by stabilizing crazes is diminished, which results in a brittle fracture mode with low extensibility. This highlights the role of ionic interactions in modulating the post-yield hardening and fracture behavior through craze formation and instability. Moreover, our results also provide into exploring and understanding the role of ionic interaction in an ionomer's failure type (brittle vs. ductile) and constitutive response and how they can be related by an appropriate analysis of a uniaxial tensile test data.

It is interesting to note that the H^+-form polymer does not follow any of the trends discussed above, implying, once again, the role of hydrogen bonds, which helps stabilize the deformation and enhance the stretchability of the polymer network. Recalling that in Section 3.3, the hydrogen bond could facilitate chain mobility and sliding, and therefore reducing deformation resistance beyond yield point. On such basis, the fracture resistance of H^+-form membrane is achieved through large plastic deformation ahead of crack tip, alleviating crack-tip stresses and exhibiting ductile fracture behavior. For other monovalent cations in the membrane, due to the large deformation resistance, plastic deformation at the head of crack tip is restricted, thereby leading to a brittle fracture pattern.

3.6 Summary: Role of Cations in Deformation

Figure 11 summarizes the properties determined from tensile and fracture tests change with cations. Of all the properties measured, with increasing cation size, Young's Modulus (E) and yield stress (Y, or PLS) increase whereas the yield strain, or strength-to-stiffness ratio (Y/E) decreases slightly. A universal relationship exists between E and Y (Figure 2), which marks the onset of nonlinearity in stress-strain curve, indicating interrelated mechanisms controlling the elasticity and yielding through the ionic interactions. As for the parameters representing large-deformation, larger cations enhance resistance to plastic flow thereby increasing the strain-hardening (G_T), while reducing the break strain, ε_{break}, and increasing craze instability (Y/G_T). In fact, increase in instability in the presence of metal alkali cations are linked to change in fracture mode. In H^+-form, Nafion exhibit ductile deformation with high fracture toughness and energy dissipation, which is similar to H-bond driven increase in toughness observed in hydrogels.[103, 104, 116, 117] Upon replacing H^+ with other metal alkali cations, Nafion exhibit similar ratio of yielding to tearing with features that are more indicative of brittle fracture, which also limits extensibility. These correlations across the deformation regimes explain the origins of the inverse relationships between extensibility and stiffness (E vs. ε_{break}, Figure 6), and between fracture toughness (w_f, βw_p) and craze/necking instability (Y/G_T), governed by ionic interactions (Figure 3). While these are seemingly semi-empirical relations, they nevertheless provide physical insights into the nature of (in)stability in polymers. In fact, changes in fracture behavior in the presence of cations were previously observed for sulfonated polystyrene[67, 69, 70] and hydrogels,[61, 63-66] but this study unravels the impact of cations on both deformation and fracture of PFSAs. To better delineate mechanisms during deformation, E, PLS and G_T are normalized relative to their values for H^+-form membrane and plotted as a function of cation radius (Figure 4), which show similar cation-dependence. The normalized G_T follows the same trend as Young's modulus (E) for monovalent cations, but deviates for multivalent cations at a

given r_c. This indicates that cation size is the predominant factor in small-strain regime, whereas for large-strain deformation, deviation in strain-hardening for multivalent cations underscores the role of ionic crosslinks in restricting the orientation of the polymer aggregates further during stretching. Even though the effect of water content on segmental dynamics cannot be ruled out completely, the overall water uptake is less than 3 water molecules per sulfonic acid group of the ionomer (Figure S3). While hydration affects the mechanical properties,[2-4, 43, 47, 49-51] for the low hydration conditions studied herein, water molecules are still strongly interacting with the ionomer moieties and can under strong influence of ionic interactions. Under such conditions, most of the water molecules are strongly interacting with, or bound to, the ionic groups and likely to be part of the hydration shell of the ions[2, 15, 17, 19, 95, 118, 119] (See ESI, Table S1). Thus, it is not trivial to separate the effect of water and effect of ions, due to the coupling among, SO_3^- ions, of water and counter-ions.

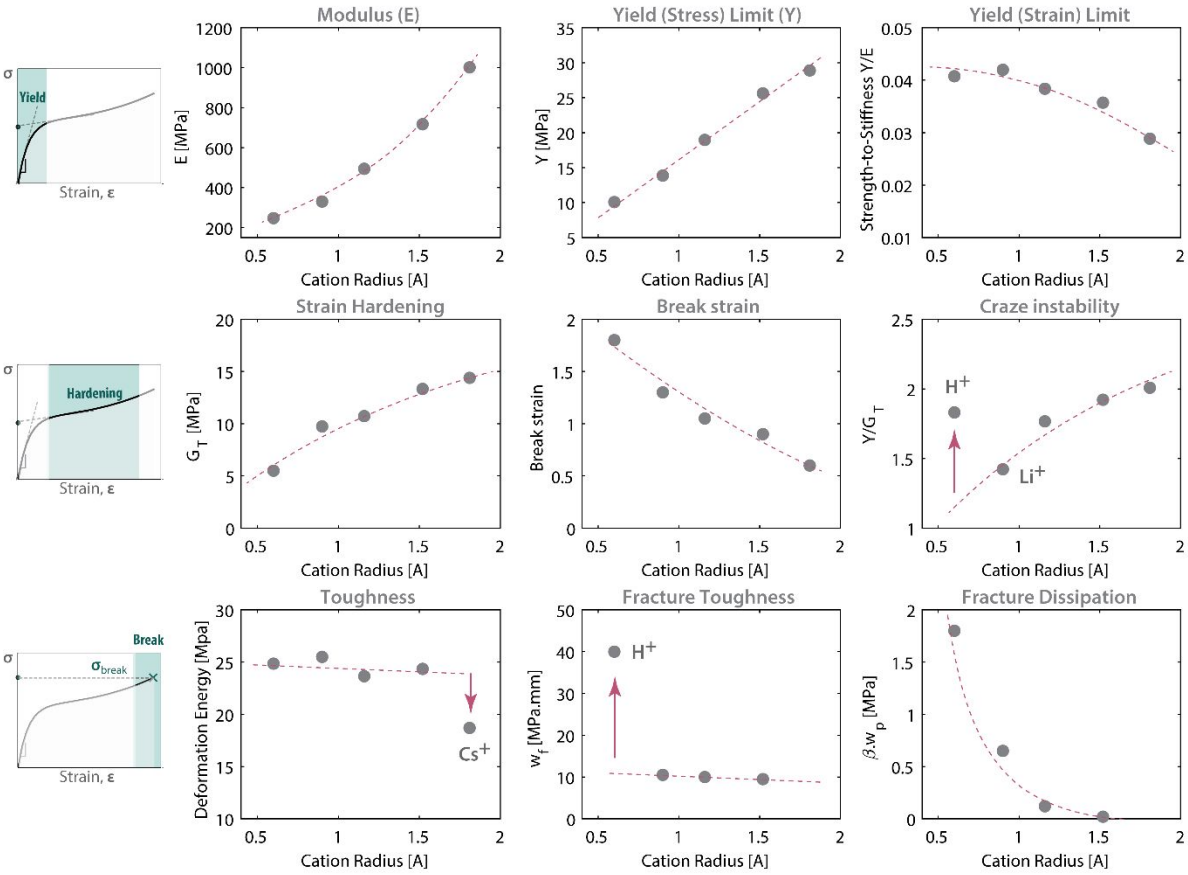

Figure 11 Comparison of measured or calculated mechanical properties of cation-exchanged Nafion membrane plotted as a function of radius of the cation in three distinct deformation modes (from top to bottom row): small-strain deformation, large-strain deformation with hardening, and fracture behavior.

In light of these findings, we posit that the constitutive model for semi-crystalline polymers (Eq. (1)) could be modified to describe the deformation behavior of cation-exchanged polymers:

ε ε ε (2)

$\varepsilon > \varepsilon_0; \sigma > Y(ion) \rightarrow$ / (3) where $\Lambda_p = 1 + \varepsilon_p = 1 + (\varepsilon - \varepsilon_0)$, and ε_0 is strain at yield (Y). The functional dependencies of *E(ion), Y(ion),* and G_T *(ion)* are due to their increase with increasing ion radius. Hardening tangent is expressed as superposition of E_r and function of cation

radius: To summarize, cations impact Nafion's mechanical behavior in three distinct deformation modes. At small-strain deformation, the ionic interactions between cations and sulfonate groups act as cross-links that reduce the mobility of the surrounding polymer chains and hinder their movement. Once the yield point is exceeded, the ionic interactions and associated physical crosslinks are disrupted partially, such that their impact on backbone-chain alignment with hardening is diminished. For small-strain deformation, higher Young's modulus and PLS of cation-exchanged membranes are induced by restricted chain mobility. For large-strain deformation after yielding, the increased strain-hardening modulus is due primarily to the larger cations with stronger interactions, thereby restricting the mobility of polymer aggregates and stabilizing the chain entanglements in the network. A secondary minor role of the cations in deformation comes from the valance effect, which creates stronger ionic crosslinks between the polymer aggregates in the network by further restricting their motion during stretching. The fact that the effective radii of multivalent cations vary in a smaller range compared to the radii of monovalent cations, allows for isolating the size and charge effects. Our results indicate that the cation size has a stronger impact on mechanical properties and deformation, than does the charge effect. The impacts of cations on deformation of ionomers are illustrated in Figure 3. These results not only confirm the suitability of the proposed constitutive model to capture large-strain deformation but also highlights the interrelation between plastic deformation with hardening and mechanical toughness through fracture energy and instability.

4. Conclusions

This study investigates the stress-strain response of Nafion membrane exchanged with cations with a focus on the underlying origins of the factors controlling the deformation and fracture mechanisms in the membrane. The measured stress-strain data are reproduced using a constitutive model, from which a set of properties is extracted and related to fracture toughness in the presence of ionic interactions. The key findings can be summarized as:

(1) For small-strain deformation, Nafion membrane's Young's moduli are impacted primarily by cation radius, whereas for large-strain deformation, the strain-hardening moduli show dependence on both cation size and charge, with a relatively smaller contribution from the latter.

(2) Below ionic-transition temperature, the membrane's Young's modulus and storage modulus are impacted significantly by the cation size, which increases the stiffness of the polymer network. However, above this temperature, the membrane enters a rubbery regime with the disintegration of its ionic network, and its rubbery modulus, E_r, does not change with cation type. Also, a linear relationship exists between Young's modulus and Yield limit, revealing the inter-dependence of deformation mechanism controlling the elasticity and yielding through the cationic interactions.

(3) The strain hardening modulus, G_T, is dependent on ionic interactions and also correlates well with the rubbery modulus, E_r. Thus, in this regime, large-strain deformation of the ionomer is governed by the alignment and stretching of polymer aggregates, in a mechanism similar to that observed in rubbery regime, but with an additional resistance caused by the ionic crosslinks formed between the cations and the polymer's sulfonate anions. This contribution can be quantitative related the cation's radius (r_c), or Lewis acid strength (LAS), leading to an expression of the form: $G_T(ion) - E_r \propto LAS \propto 1/r_c$.

(4) The elongation to break values are inversely proportional to the stiffness and strength of the membrane, regardless of the cation form, underscoring the trade-off between stretchability and stiffness, even though the membrane's strain energy density is less dependent on cations.

(5) From double-edge notch tension tests, H^+-form membrane exhibits ductile fracture mode while the rest monovalent cationic membranes exhibit brittle fracture mode. Such a change in fracture mode

is related to the increasing craze instability, which can be diminished significantly in the presence of H-bond which makes the ionomer more ductile. An inverse relationship exists between fracture toughness (w_f, βw_p) and craze/necking instability (Y/G_T), implying that fracture behavior in the presence of cations is controlled by craze instability represented by Y/G_T parameter extracted from tensile test and highlighting the role of plastic deformation and hardening in governing fracture toughness through craze formation and instability.

In conclusion, our results shed light on the effects of cations and ionic interactions in an ionomer's failure (e.g., brittle vs. ductile) and constitutive behavior, and provide insight into their interrelation can be analyzed using uniaxial tensile tests. The findings in this study delineate the role of ionic interactions in mechanical behavior and stability of Nafion and similar ionomers in both small- and large-deformation regime, which would be critical for improving the current state of understanding of stability ion-exchange membranes in emerging technologies on clean water and energy.

Acknowledgements

We would like thank Andrew Crothers and Dr. Douglas Kushner of Berkeley Lab for their insightful reading of the manuscript. SS, ZL, QL and XC gratefully acknowledge the financial support from the National Natural Science Foundation of China (No.51805364). Funding for this work was provided by the Fuel Cell Technologies Office (FCTO), Office of Energy Efficiency and Renewable Energy (EERE), of the U.S. Department of Energy under contract number DE-AC02-05CH11231.

References

1. M. L. Perry and A. Z. Weber, *J. Electrochem. Soc.*, 2016, **163**, A5064-A5067.
2. A. Kusoglu and A. Z. Weber, *Chem Rev*, 2017, **117**, 987-1104.
3. A. Kusoglu, S. Savagatrup, K. T. Clark and A. Z. Weber, *Macromolecules*, 2012, **45**, 7467-7476.
4. S. W. Shi, A. Z. Weber and A. Kusoglu, *Electrochim. Acta*, 2016, **220**, 517-528.
5. W. Xie, R. M. Darling and M. L. Perry, *J. Electrochem. Soc.*, 2016, **163**, A5084-A5089.
6. G. Alberti, R. Narducci and M. Sganappa, *J. Power Sources*, 2008, **178**, 575-583.
7. S. Shi, T. J. Dursch, C. Blake, R. Mukundan, R. L. Borup, A. Z. Weber and A. Kusoglu, *J. Polym. Sci., Part B: Polym. Phys.*, 2016, **54**, 570-581.
8. R. Mukundan, A. M. Baker, A. Kusoglu, P. Beattie, S. Knights, A. Z. Weber and R. L. Borup, *J. Electrochem. Soc.*, 2018, **165**, F3085-F3093.
9. F. D. Coms, S. Schlick and M. Danilczuk, in *The Chemistry of Membranes Used in Fuel Cells*, 2017, DOI: 10.1002/9781119196082.ch4, pp. 75-106.
10. K. A. Page, K. M. Cable and R. B. Moore, *Macromolecules*, 2005, **38**, 6472-6484.
11. A. K. Phillips and R. B. Moore, *J. Polym. Sci., Part B: Polym. Phys.*, 2006, **44**, 2267-2277.
12. T. Okada, H. Satou, M. Okuno and M. Yuasa, *J. Phys. Chem. B*, 2002, **106**, 1267-1273.
13. E. Negro, M. Vittadello, K. Vezzu, S. J. Paddison and V. Noto, *Solid State Ionics*, 2013, **252**, 84-92.
14. E. Moukheiber, C. Bas, N. D. Alberola and L. Flandin, *J. Membr. Sci.*, 2013, **431**, 105-112.
15. A. Münchinger and K.-D. Kreuer, *J. Membr. Sci.*, 2019, **592**.
16. H. L. Yeager and A. Steck, *Anal Chem*, 1979, **51**, 862-865.
17. A. Steck and H. L. Yeager, *Anal Chem*, 1980, **52**, 1215-1218.
18. T. D. Gierke, G. E. Munn and F. C. Wilson, *J. Polym. Sci., Part B: Polym. Phys.*, 1981, **19**, 1687-1704.
19. H. L. Yeager and A. Steck, *J. Electrochem. Soc.*, 1981, **128**, 1880-1884.
20. J. R. Bontha and P. N. Pintauro, *Chem. Eng. Sci.*, 1994, **49**, 3835-3851.
21. T. Okada, S. Moller-Holst, O. Gorseth and S. Kjelstrup, *J. Electroanal. Chem.*, 1998, **442**, 137-145.
22. R. Tandon and P. N. Pintauro, *J. Membr. Sci.*, 1997, **136**, 207-219.
23. S. Quezado, J. C. T. Kwak and M. Falk, *Can J Chem*, 1984, **62**, 958-966.

24. Y. F. Fan, D. Tongren and C. J. Cornelius, *Eur Polym J*, 2014, **50**, 271-278.
25. S. Chaudhury, C. Agarwal, A. K. Pandey and A. Goswami, *J. Phys. Chem. B*, 2012, **116**, 1605-1611.
26. R. Tandon and P. N. Pintauro, *J. Membr. Sci.*, 2009, **341**, 21-29.
27. A. R. Crothers, C. J. Radke and A. Z. Weber, *ECS Trans.*, 2017, **80**, 593-604.
28. E. Negro, M. Vittadello, K. Vezzù, S. J. Paddison and V. Di Noto, *Solid State Ionics*, 2013, **252**, 84-92.
29. S. R. Lowry and K. A. Mauritz, *Journal of the American Chemical Society*, 1980, **102**, 4665-4667.
30. T. Kyu and A. Eisenberg, *Journal of Polymer Science: Polymer Symposia*, 1984, **71**, 203-219.
31. K. M. Cable, K. A. Mauritz and R. B. Moore, *J. Polym. Sci., Part B: Polym. Phys.*, 1995, **33**, 1065-1072.
32. T. Kyu and A. Eisenberg, *J Polym Sci Pol Sym*, 1984, **71**, 203-219.
33. S. Kundu, L. C. Simon, M. Fowler and S. Grot, *Polymer*, 2005, **46**, 11707-11715.
34. G. Suresh, A. K. Pandey and A. Goswami, *J. Membr. Sci.*, 2006, **284**, 193-197.
35. N. H. Jalani and R. Datta, *J. Membr. Sci.*, 2005, **264**, 167-175.
36. M. Saito, N. Arimura, K. Hayamizu and T. Okada, *J. Phys. Chem. B*, 2004, **108**, 16064-16070.
37. M. Legras, Y. Hirata, Q. T. Nguyen, D. Langevin and M. Métayer, *Desalination*, 2002, **147**, 351-357.
38. Y. Fan, D. Tongren and C. J. Cornelius, *European Polymer Journal*, 2014, **50**, 271-278.
39. S. Chaudhury, C. Agarwal and A. Goswami, *J. Phys. Chem. B*, 2015, **119**, 10566-10572.
40. K. Hongsirikarn, J. G. Goodwin Jr, S. Greenway and S. Creager, *J. Power Sources*, 2010, **195**, 7213-7220.
41. A. Goswami, A. Acharya and A. K. Pandey, *J. Phys. Chem. B*, 2001, **105**, 9196-9201.
42. A. Kusoglu, Y. Tang, M. H. Santare, A. M. Karlsson, S. Cleghorn and W. B. Johnson, *J Fuel Cell Sci Tech*, 2009, **6**, 011012-011018.
43. A. Kusoglu, Y. L. Tang, M. Lugo, A. M. Karlsson, M. H. Santare, S. Cleghorn and W. B. Johnson, *J. Power Sources*, 2010, **195**, 483-492.
44. Y. L. Tang, A. M. Karlsson, M. H. Santare, M. Gilbert, S. Cleghorn and W. B. Johnson, *Mat Sci Eng a-Struct*, 2006, **425**, 297-304.
45. D. Liu, S. Kyriakides, S. W. Case, J. J. Lesko, Y. X. Li and J. E. McGrath, *J. Polym. Sci., Part B: Polym. Phys.*, 2006, **44**, 1453-1465.

46. Y. Kawano, T. Wang, R. A. Palmer and S. R. Aubuchon, *Polímeros: Ciência e Tecnologia*, 2002, **12**, 96-101.

47. S. Shi, D. Liu, D. Liu, P. Tae, C. Y. Gao, L. Yan, K. An and X. Chen, *Polym. Eng. Sci.*, 2014, **54**, 2215-2221.

48. Z. W. Lu, M. H. Santare, A. M. Karlsson, F. C. Busby and P. Walsh, *J. Power Sources*, 2014, **245**, 543-552.

49. A. Kusoglu, M. H. Santare, A. M. Karlsson, S. Cleghorn and W. B. Johnson, *J. Polym. Sci., Part B: Polym. Phys.*, 2008, **46**, 2404-2417.

50. A. Kusoglu, Y. L. Tang, M. H. Santare, A. M. Karlsson, S. Cleghorn and W. B. Johnson, *J Fuel Cell Sci Tech*, 2009, **6**, 011012-011018.

51. N. S. Khattra, A. M. Karlsson, M. H. Santare, P. Walsh and F. C. Busby, *J. Power Sources*, 2012, **214**, 365-376.

52. Y. Kawano, Y. Wang, R. A. Palmer and S. R. Aubuchon, *Polímeros*, 2002, **12**, 96-101.

53. S. Kundu, L. C. Simon, M. Fowler and S. Grot, *Polymer*, 2005, **46**, 11707-11715.

54. R. L. Jia, B. H. Han, K. Levi, T. Hasegawa, J. P. Ye and R. H. Dauskardt, *J. Power Sources*, 2011, **196**, 3803-3809.

55. R. Jia, S. Dong, T. Hasegawa, J. Ye and R. H. Dauskardt, *Int. J. Hydrogen Energy*, 2012, **37**, 6790-6797.

56. S. C. Yeo and A. Eisenberg, *J. Appl. Polym. Sci.*, 1977, **21**, 875-898.

57. K. B. Daly, A. Z. Panagiotopoulos, P. G. Debenedetti and J. B. Benziger, *J. Phys. Chem. B*, 2014, **118**, 13981-13991.

58. Y. Q. Li, J. K. Quincy, S. W. Case, M. W. Ellis, D. A. Dillard, Y. H. Lai, M. K. Budinski and C. S. Gittleman, *J. Power Sources*, 2008, **185**, 374-380.

59. K. Patankar, D. A. Dillard, S. W. Case, M. W. Ellis, Y. Q. Li, Y. H. Lai, M. K. Budinski and C. S. Gittleman, *J. Polym. Sci., Part B: Polym. Phys.*, 2010, **48**, 333-343.

60. D. Basu, A. Das, K. W. Stockelhuber and S. Wiessner, *Designing of Elastomer Nanocomposites: From Theory to Applications*, 2017, **275**, 235-266.

61. S. Naficy, S. Kawakami, S. Sadegholvaad, M. Wakisaka and G. M. Spinks, *J. Appl. Polym. Sci.*, 2013, **130**, 2504-2513.

62. J. Y. Sun, X. H. Zhao, W. R. K. Illeperuma, O. Chaudhuri, K. H. Oh, D. J. Mooney, J. J. Vlassak and Z. G. Suo, *Nature*, 2012, **489**, 133-136.

63. J. S. Lee, H. S. Park, Y. J. Kim and J. H. Kim, *J. Appl. Polym. Sci.*, 2018, **135**.

64. M. Sarker, M. Izadifar, D. Schreyer and X. Chen, *J Biomater Sci Polym Ed*, 2018, **29**, 1126-1154.

65. B. Y. Zhang, Z. J. Gao, G. H. Gao, W. Zhao, J. S. Li and X. Y. Ren, *Macromol Mater Eng*, 2018, **303**.

66. Z. H. Qin, R. Niu, C. J. Tang, J. Xia, F. Ji, D. Y. Dong, H. T. Zhang, S. Zhang, J. J. Li and F. L. Yao, *Macromol Mater Eng*, 2018, **303**.

67. M. A. Bellinger, J. A. Sauer and M. Hara, *Polymer*, 1994, **35**, 5478-5482.

68. M. Hara, M. Bellinger and J. A. Sauer, *Colloid. Polym. Sci.*, 1992, **270**, 652-658.

69. M. Hara, M. Bellinger and J. A. Sauer, *Polym. Int.*, 1991, **26**, 137-141.

70. M. Hara, P. Jar and J. A. Sauer, *Polymer*, 1991, **32**, 1622-1626.

71. S. K. Young, S. F. Trevino, N. C. B. Tan and R. L. Paul, *J. Polym. Sci., Part B: Polym. Phys.*, 2003, **41**, 1485-1492.

72. Q. Lin, Z. Liu, L. Wang, X. Chen and S. Shi, *J. Power Sources*, 2018, **398**, 34-41.

73. P. Van der Heijden, L. Rubatat and O. Diat, *Macromolecules*, 2004, **37**, 5327-5336.

74. L. Rubatat and O. Diat, *Macromolecules*, 2007, **40**, 9455-9462.

75. S. A. Visser and S. L. Cooper, *Macromolecules*, 1992, **25**, 2230-2236.

76. J. K. Park, J. Li, G. M. Divoux, L. A. Madsen and R. B. Moore, *Macromolecules*, 2011, **44**, 5701-5710.

77. V. Barbi, S. S. Funari, R. Gehrke, N. Scharnagl and N. Stribeck, *Polymer*, 2003, **44**, 4853-4861.

78. P. C. van der Heijden, L. Rubatat and O. Diat, *Macromolecules*, 2004, **37**, 5327-5336.

79. K. M. Cable, K. A. Mauritz and R. B. Moore, *Chem Mater*, 1995, **7**, 1601-1603.

80. J. Li, J. K. Park, R. B. Moore and L. A. Madsen, *Nat Mater*, 2011, **10**, 507-511.

81. Z. W. Lu, M. Lugo, M. H. Santare, A. M. Karlsson, F. C. Busby and P. Walsh, *J. Power Sources*, 2012, **214**, 130-136.

82. Y. Tang, A. M. Karlsson, M. H. Santare, M. Gilbert, S. Cleghorn and W. B. Johnson, *Mater. Sci. Eng., A*, 2006, **425**, 297-304.

83. Z. Lu, M. Lugo, M. H. Santare, A. M. Karlsson, F. C. Busby and P. Walsh, *J. Power Sources*, 2012, **214**, 130-136.

84. R. N. Haward and G. Thackray, *Proceedings of the Royal Society of London. Series A. Mathematical and Physical Sciences*, 1968, **302**, 453-472.

85. R. N. Haward, *Polymer*, 1987, **28**, 1485-1488.

86. A. Frick, D. Sich, G. Heinrich, C. Stern, M. Gossi and T. A. Tervoort, *Macromol Mater Eng*, 2013, **298**, 954-966.

87. R. N. Haward, *Macromolecules*, 1993, **26**, 5860-5869.

88. P. J. Rae and E. N. Brown, *Polymer*, 2005, **46**, 8128-8140.

89. G. Xie and T. Okada, *J. Electrochem. Soc.*, 1995, **142**, 3057-3062.

90. T. Okada, G. Xie, O. Gorseth, S. Kjelstrup, N. Nakamura and T. Arimura, *Electrochim. Acta*, 1998, **43**, 3741-3747.

91. K.-D. Kreuer, S. J. Paddison, E. Spohr and M. Schuster, *Chem. Rev.*, 2004, **104**, 4637-4678.

92. S. R. Lowry and K. A. Mauritz, *J. Am. Chem. Soc.*, 1980, **102**, 4665-4667.

93. A. L. Rollet, G. Gebel, J. P. Simonin and P. Turq, *J. Polym. Sci., Part B: Polym. Phys.*, 2001, **39**, 548-558.

94. A. R. Crothers, *J. Electrochem. Soc.*, 2019, **under review**.

95. M. Falk, *Can. J. Chem.*, 1980, **58**, 1495-1501.

96. J. P. G. Villaluenga, V. M. Barragan, B. Seoane and C. Ruiz-Bauza, *Electrochim. Acta*, 2006, **51**, 6297-6303.

97. K. A. Page, F. A. Landis, A. K. Phillips and R. B. Moore, *Macromolecules*, 2006, **39**, 3939-3946.

98. K. A. Page, J. K. Park, R. B. Moore and V. G. Sakai, *Macromolecules*, 2009, **42**, 2729-2736.

99. E. Moukheiber, G. De Moor, L. Flandin and C. Bas, *J. Membr. Sci.*, 2012, **389**, 294-304.

100. K. A. Patankar, D. A. Dillard, S. W. Case, M. W. Ellis, Y. H. Lai, M. K. Budinski and C. S. Gittleman, *Mech. Time-Depend. Mater.*, 2008, **12**, 221-236.

101. K. A. Patankar, D. A. Dillard, S. W. Case, M. W. Ellis, Y. H. Lai and C. S. Gittleman, *Fuel Cells*, 2012, **12**, 787-799.

102. C. Bas, L. Reymond, A. S. Danerol, N. D. Alberola, E. Rossinot and L. Flandin, *J. Polym. Sci., Part B: Polym. Phys.*, 2009, **47**, 1381-1392.

103. X. B. Hu, J. Zhou, W. F. M. Daniel, M. Vatankhah-Varnoosfaderani, A. V. Dobrynin and S. S. Sheiko, *Macromolecules*, 2017, **50**, 652-659.

104. X. N. Zhang, Y. J. Wang, S. T. Sun, L. Hou, P. Y. Wu, Z. L. Wu and Q. Zheng, *Macromolecules*, 2018, **51**, 8136-8146.

105. H. G. H. van Melick, L. E. Govaert and H. E. H. Meijer, *Polymer*, 2003, **44**, 2493-2502.

106. R. O. Ritchie, *Nat Mater*, 2011, **10**, 817-822.

107. M. E. Launey and R. O. Ritchie, *Adv Mater*, 2009, **21**, 2103-2110.

108. S. J. Lee, H. M. Yang, K. G. Cho, K. H. Seol, S. Kim, K. Hong and K. H. Lee, *Org Electron*, 2019, **65**, 426-433.

109. Y. S. Kim, C. F. Welch, R. P. Hjelm, N. H. Mack, A. Labouriau and E. B. Orler, *Macromolecules*, 2015, **48**, 2161-2172.

110. E. Moukheiber, C. Bas and L. Flandin, *Int. J. Hydrogen Energy*, 2014, **39**, 2717-2723.

111. R. N. Haward, *Macromolecules*, 1993, **26**, 5860-5869.

112. E. J. Kramer and L. L. Berger, in *Crazing in Polymers Vol. 2*, ed. H. Kausch, Springer Berlin / Heidelberg, 1990, vol. 91, ch. Chapter 1, pp. 1-68.

113. A. M. Donald and E. J. Kramer, *J. Polym. Sci., Part B: Polym. Phys.*, 1982, **20**, 899-909.

114. T. N. Krupenkin and G. H. Fredrickson, *Macromolecules*, 1999, **32**, 5036-5045.

115. T. N. Krupenkin and G. H. Fredrickson, *Macromolecules*, 1999, **32**, 5029-5035.

116. X. F. Li, M. M. Shu, H. Li, X. Gao, S. J. Long, T. Hu and C. G. Wu, *Rsc Adv*, 2018, **8**, 16674-16689.

117. X. Hu, M. Vatankhah-Varnoosfaderani, J. Zhou, Q. Li and S. S. Sheiko, *Adv Mater*, 2015, **27**, 6899-6905.

118. A. Eisenberg, *Macromolecules*, 1970, **3**, 147 - 154.

119. E. Glueckauf, *T Faraday Soc*, 1955, **51**, 1235-1244.

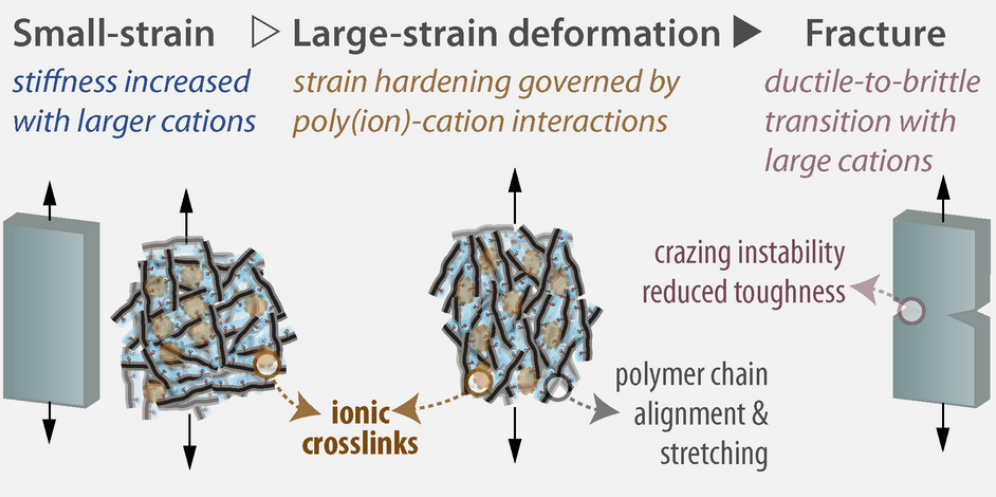

79x39mm (300 x 300 DPI)